

The second decametre pulsar census at UTR-2 radio telescope

Ihor P. Kravtsov,¹★ Vyacheslav V. Zakharenko,^{1,2} Oleg M. Ulyanov,¹ Alisa I. Shevtsova,¹
Serge M. Yerin,^{1,2} Oleksandr. O. Konovalenko¹

¹*Institute of Radio Astronomy of NAS of Ukraine, 4 Mystetstv st., 61002, Kharkiv, Ukraine*

²*V. N. Karazin Kharkiv National University, 4 Svobody Sq., 61022, Kharkiv, Ukraine*

Accepted XXX. Received YYY; in original form ZZZ

ABSTRACT

Our paper presents the results of the second census of pulsars in decametre wave range at UTR-2 radio telescope. Over the past ten years, the number of discovered nearby pulsars in the world has doubled, which has made it urgent to search for a low-frequency radio emission from newly discovered sources. To increase this census sensitivity, the integration time was doubled compared with the first census of 2010–2013. As a result, the decametre radio emission of 20 pulsars was detected, their flux densities and the shape of pulses were obtained. The dispersion measure for 10 pulsars and the rotation period for 8 pulsars were refined. For several pulsars the scattering time constant and FWHM were estimated in decametre wave range. Upper limits of flux densities of 102 not yet detected pulsars were also estimated.

Key words: methods: data analysis – pulsars: general – pulsars: individual: PSR J1426+52

1 INTRODUCTION

Pulsars were discovered more than 50 years ago (Hewish et al. 1968) however, the interest in studying them is constantly growing due to their importance for studies of interstellar medium, stellar evolution, high-energy physics and possible gravitational waves sensing.

Due to the development of radio astronomical observation techniques and data processing tools (as well as ongoing efforts in search for new sources), the number of discovered pulsars is constantly increasing. The maximum flux of these sources' radiation lays in the meter wave range, that means the new searches of nearby sources in the frequency range below 1 GHz are quite promising. A lot of new instruments have been introduced in this range recently. Among them UTMOST (upgraded telescope Molongo Observatory Synthesis Telescope) (Bailes et al. 2017), LWA (Long Wavelength Array) (Stovall et al. 2015), NenuFAR (New Extension in Nançay Upgrading LOFAR) (Zarka et al. 2015) can be named. The most anticipated in the whole radio range is the introduction of SKA (Square Kilometer Array) (Keane et al. 2014).

For the extremely low frequencies (10–30 MHz), the strong increase in the scattering time of pulsar pulses with a frequency decreasing ($\propto \nu^{-4.4}$) makes it impossible to study the pulsed radiation of distant pulsars. These studies are further complicated by factors such as: (i) larger dispersion delay comparing to its values at high frequencies ($\propto f^{-2}$), (ii) increase in the background brightness temperature of the Galaxy ($\propto f^{-2.55}$) (Lawson et al. 1987), (iii) growing power and number of terrestrial radio frequency interference sources.

However, for nearby pulsars with dispersion measures (DM) up to 30 pc cm^{-3} , which correspond to a distance of 1–2 kpc (depending on the pulsar galactic coordinates), the number of pulsars detected before 2010 in the decametre wave range (about a dozen) seemed

very small. Deep upgrade of the UTR-2 radio telescope and its receiving system (Konovalenko et al. 2016; Zakharenko et al. 2016) allowed to increase this number. It turned out that for effective pulsar detection in the decametre wave range, the DM values obtained from high frequency data in some cases are not accurate enough. Refinement of the DM values during data processing, maximal use of the bandwidth and radio frequency interference (RFI) mitigation in the first decametre pulsar census (2010–2013) allowed authors to detect 40 of 74 known at that time pulsars with parameters: rotation period (P) longer than 0.1 s, DM less than 30 pc cm^{-3} , declinations (δ or dec) above -10° (Zakharenko et al. 2013).

The first decametre survey of pulsars and sporadic radiation sources of the Northern sky (Vasylieva et al. 2013; Vasylieva 2015; Kravtsov et al. 2016a,b,c; Zakharenko et al. 2018) revealed a large number of bursts originating from space (non-repeating pulses that look like pulsar emission). Some of the bursts could be single (anomalously intense) pulses (Ulyanov et al. 2006; Ulyanov & Zakharenko 2012) of hitherto unknown pulsars, but to compare and reliably identify these pulses with known sources, it is necessary to determine their radiation parameters with sufficient accuracy. For example, the DM value must be measured with an accuracy of 0.01 pc cm^{-3} or higher.

In the last decade the number of the new pulsars with parameters suitable for observations at the UTR-2 has doubled, especially due to such surveys as the LOTAAS (at LOFAR) (Sanidas et al. 2019) and the GBT pulsar survey (at the Green Bank Telescope) (Kawash et al. 2018). The new discoveries demanded a new census of pulsars in the decametre wave range both to expand the list of studied sources and to potentially identify the discovered transient signals with the individual pulses of new pulsars.

★ E-mail: i.p.kravtsov@gmail.com (KTS)

2 INSTRUMENTATION AND OBSERVATIONS

For pulsar observations at the UTR-2 radio telescope (Konvalenko et al. 2016) we used the sum of “North – South” and “East – West” antennas’ signals mode. This mode provides the highest sensitivity, while the confusion effect during the pulsar search is not dangerous. In contrast to the first decametre pulsar census (Zakharenko et al. 2013), when the question of the possibility of detecting the radiation of a large number of pulsars at UTR-2 was actually relevant, in this work we pay more attention to the sensitivity increasing by means of increasing the integration time from 1.5 hours in the previous census to 3 hours in the current one. As in Zakharenko et al. (2013), a range of dispersion measures is $0 \pm 30 \text{ pc cm}^{-3}$ with a step of 0.002 pc cm^{-3} in 16.5–33.0 MHz frequency range (4096 channels with $\approx 4 \text{ kHz}$ width) was chosen. Since the scattering time constant in the decametre wave range for majority of known pulsars (even the nearest ones) exceeds 10 ms, we use a time resolution of 8 ms, a post-detector method of dedispersion and an advanced (in comparison with Zakharenko et al. 2013) RFI mitigation procedure (Vasylyeva et al. 2013; Vasylyeva 2015).

As of the beginning of 2020, 163 pulsars which meet the abovementioned criteria ($DM < 30 \text{ pc cm}^{-3}$, $P > 0.1 \text{ s}$, $\delta > -10^\circ$) were known from the primary sources (see Kravtsov et al. 2020, and references there) and from the ATNF pulsar catalogue (Manchester et al. 2005). Forty of these pulsars were detected during the first census, another one (PSR J0242+62) was detected later (Vasylyeva et al. 2014). Therefore, in this work we observed 122 pulsars, which have not been detected at decametre waves yet. Note that some characteristics of a number of recently discovered pulsars has not been determined (flux density, scattering time constant, etc.) or has not been measured accurately enough. Among these parameters the main one is the pulsar period therefore it was taken as a tunable parameter for some pulsars during their search.

As an example of observational data processing of a pulsar with poor rotational period accuracy we can show the PSR J1426+52 before our refinement (Fig. 1) and successful detection after the period refinement (Fig. 2). The rotation period of PSR J1426+52 reported in Sanidas et al. (2019) has only four significant digits (0.9958 s), so its accuracy is rather low, same as for dozens of other recently discovered pulsars. Using of this rough rotation period value gave the result shown in Fig. 1.

One should note that the “DM – rotational phase” plot has light inclined oval centered at 0.48 on the x-axis and 0.18 pc cm^{-3} – on y-axis. With clarifying the pulsar period with coarse (10^{-5} s) and fine (10^{-6} s) steps to speed up calculations, we detected PSR J1426+52 with the maximal signal-to-noise ratio (S/N) of about 17 and the narrowest average pulse profile with $P = 0.995866 \text{ s}$ (Kravtsov et al. 2020).

Another example of rotational period refinement is PSR J0121+14. It was detected in the daytime (its culmination on February 10, 2020 was around 15:30 local time). The measured DM value is 17.69 pc cm^{-3} (hereinafter the error in DM determination obtained when the S/N falls to 0.95 from the maximal value) and does not differ from that obtained in Sanidas et al. (2019) ($DM = 17.77 \text{ pc cm}^{-3}$). We have also refined the pulsar period (our value $P = 1.388993 \text{ s}$, see Fig. 3) which was indicated with lower accuracy in Sanidas et al. (2019) a 1.3890 s. Some time later, in Michilli et al. (2020) rotational period of this source was measured with high accuracy ($P = 1.38899395038 \text{ s}$). Our rotational period value completely coincides with the high-precision measurements from Michilli et al. (2020) (taking into account our restriction described at the beginning of the Section 3), which confirms the reliability of our refinement of

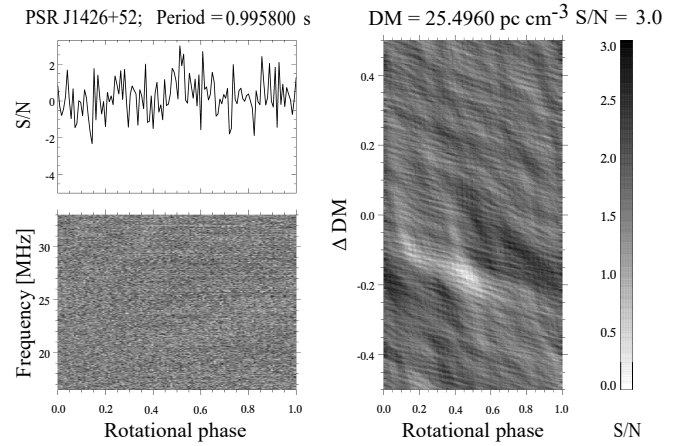


Figure 1. Results of PSR J1426+52 data processing with the rough period value $P = 0.9958 \text{ s}$ (hereinafter intensity is normalized to the off-pulse noise). The upper left panel shows an average pulse profile, the lower left one – its average spectrum. The right panel shows “dispersion measure – rotational phase” plot, as in Zakharenko et al. (2013), which helps to refine the DM value.

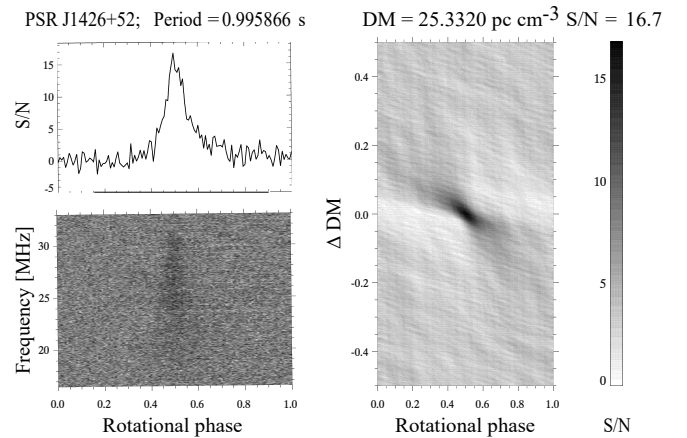


Figure 2. Results of detection of PSR J1426+52 with the refined period value $P = 0.995866 \text{ s}$.

the rotational period using the criterion for maximizing the S/N and obtaining the narrowest possible pulse profile of the pulsar. Since PSR J0121+14 is quite a powerful source, we also succeeded to estimate its scattering time constant, which is $\tau_{sc} = 51 \pm 16 \text{ ms}$. Scattering time constant was determined following Zakharenko et al. (2013) by fitting the intensity decrease versus time in the pulse tail by a law $\propto e^{-t/\tau_{sc}}$, assuming a rectangular shape for the pulse.

In order to optimize the observation time at the UTR-2 radio telescope, the observation sessions each time included a set of pulsars with culmination times spaced by about 3 hours from one another. Such pulsar selection provides maximal use of the UTR-2 effective area, because each source was recorded close to its culmination. However, observations of the majority of pulsars were carried out in the morning, afternoon and evening, i.e. in suboptimal interference conditions. Note that in the first census about 60% of observations were made during the daytime, which in the presence of a strong RFI in the decametre wave range could be an obstacle to the detection of a significant number of pulsars. In this work, the pulsars were observed

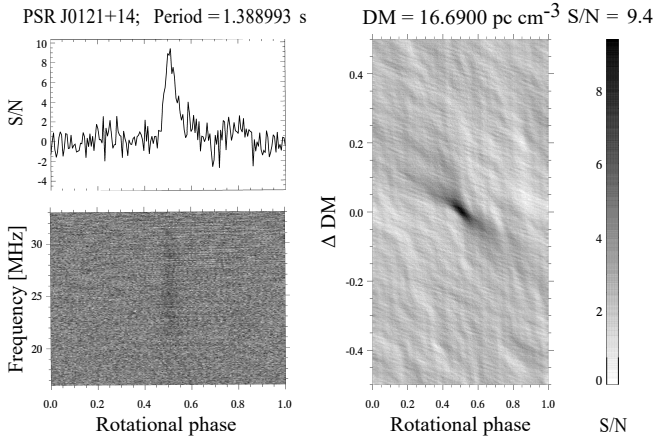


Figure 3. Results of PSR J0121+14 detection on February 10, 2020 with the refined rotation period $P = 1.388993$ s.

in a period from February 2020 to February 2021 (February 3-17, May 25-June 1, September 7-14, November 16-23 and December 21-26 – in 2020 and February 8-15, 2021).

3 RESULTS AND DISCUSSION

As a result of the work, the decametre radio emission of 20 pulsars has been detected. For 16 pulsars, the values of their DMs have been refined. In 8 cases, the period was refined up to the sixth significant digit (based on the ratio of time resolution and duration of observations: $0.008 \text{ s} / 10800 \text{ s} = 7.4 \cdot 10^{-7}$). For some pulsars, the scattering time constant at the central frequency of the range (24 MHz) has been determined. We provide the data for each pulsar below.

3.1 Average pulse profile and pulsar parameters

PSR J0121+14. We have already shown this pulsar in Section 2 (see Fig. 3) as an example of period refinement, we found its $P = 1.388993$ s and $\text{DM} = 17.69 \pm 0.02 \text{ pc cm}^{-3}$.

PSR B0301+19 was detected with a low S/N of about 5 (Fig. 4). It correlates well with the results of Zakharenko et al. (2013), where 1.5-hour observations did not result in this pulsar radio emission detection above the level (4σ). This result allows us to compare the sensitivity of the two decametre pulsar censuses and to estimate the upper detection limit (see paragraph 3.2 in Zakharenko et al. 2013). We measured the DM to be $15.659 \pm 0.020 \text{ pc cm}^{-3}$, taking into account the error, it does not differ from the value $15.65677 \pm 0.00035 \text{ pc cm}^{-3}$ specified in Bilous et al. (2016).

PSR J0317+13. When we processed the data of PSR J0317+13 with parameters given in Sanidas et al. (2019), namely the period $P = 1.9743$ s and the $\text{DM} = 12.90 \pm 0.04 \text{ pc cm}^{-3}$, we were not able to detect this pulsar. However, the period value variation with a step of 0.00001 s led to a weak detection of an average pulse profile at $P = 1.97440$ s (Fig. 5) and allowed us to refine the DM to $13.148 \pm 0.020 \text{ pc cm}^{-3}$.

PSR J0454+45. We used $P = 1.3891369360$ s and $\text{DM} = 20.834 \pm 0.002 \text{ pc cm}^{-3}$ from Tan et al. (2020) to process the data and obtained the average profile shown in Fig. 6. We estimated the $\text{DM} = 20.854 \pm 0.020 \text{ pc cm}^{-3}$ which is very close to the values from the paper.

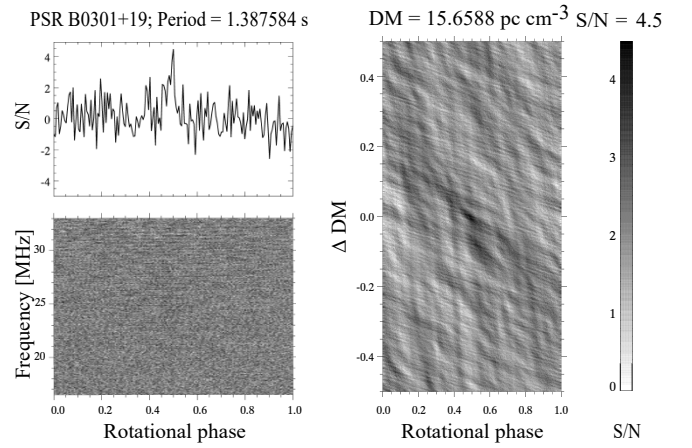


Figure 4. Results of PSR B0301+19 detection on February 5, 2020.

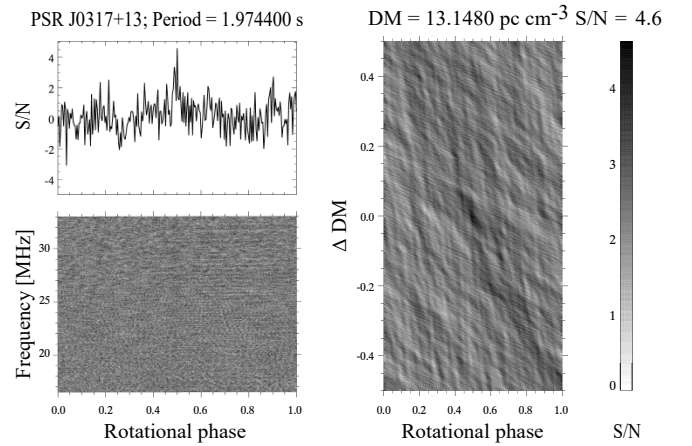


Figure 5. Results of PSR J0317+13 detection on February 16, 2020 with the refined rotation period $P = 1.97440$ s.

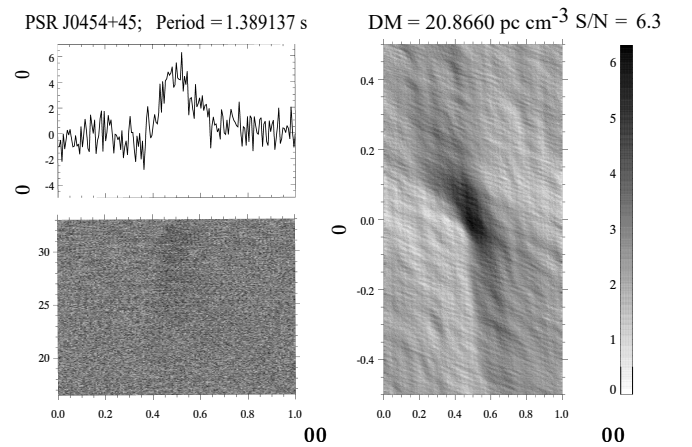


Figure 6. Detection of PSR J0454+45 on February 8, 2021.

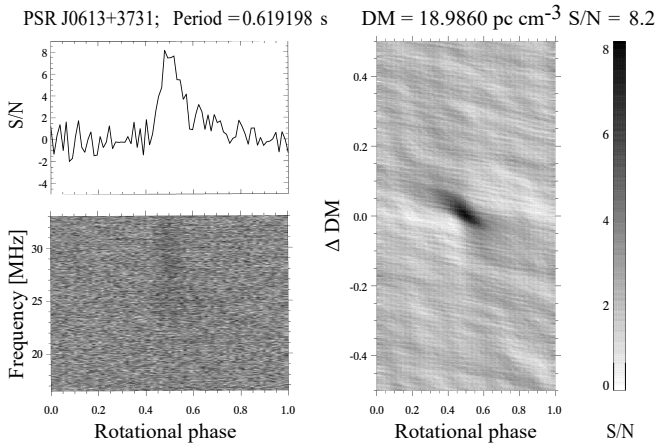


Figure 7. Detection of PSR J0613+3731 on November 19, 2020.

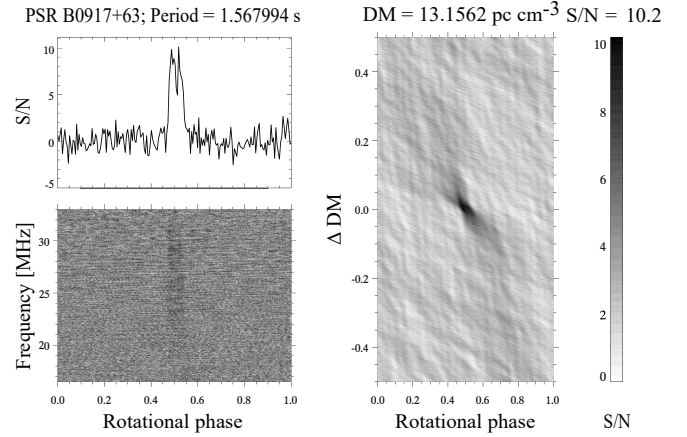


Figure 9. Detection of PSR B0917+63 on May 28, 2020.

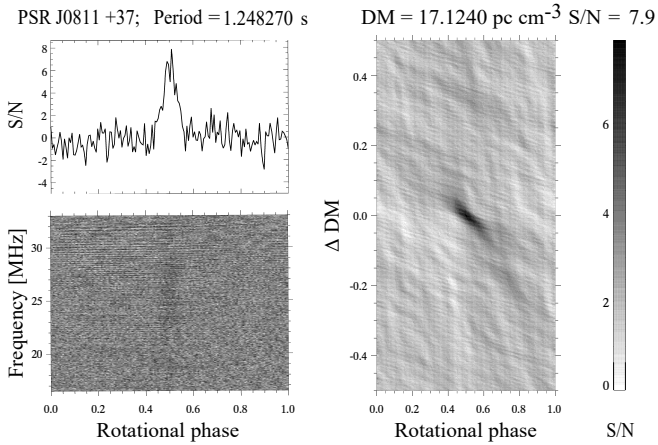


Figure 8. Detection of PSR J0811+37 on February 9, 2020 with the refined rotation period $P = 1.24827$ s.

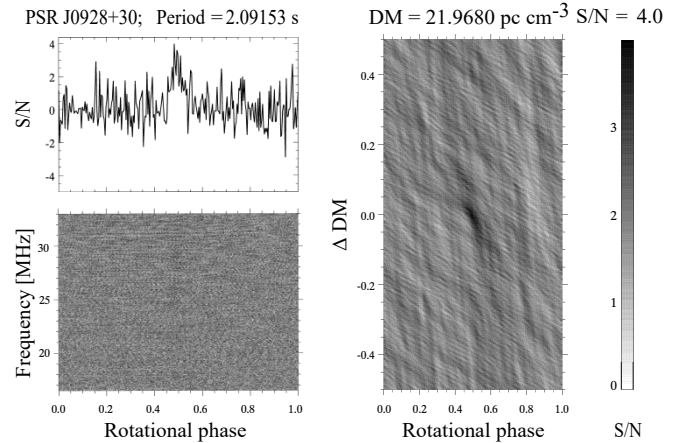


Figure 10. Detection of PSR J0928+30 on February 9, 2021 with the refined rotation period $P = 2.09153$ s.

PSR J0613+3731 was observed three times during the year: in February, September and November 2020. The third session resulted in the most reliable detection ($S/N > 8$) due to the most suitable for observations season of the year and culmination local time at about 1h 50m. Our average pulse profile (Fig. 7) allowed us to refine the $DM = 18.986 \pm 0.020$ pc cm $^{-3}$ which almost equals to the one specified in Tan et al. (2020) (18.990 ± 0.012 pc cm $^{-3}$) taking errors into account. We also estimated the pulse's scattering time constant, which is $\tau_{sc} = 30 \pm 10$ ms.

PSR J0811+37. We used initial parameters $DM = 16.95 \pm 0.11$ pc cm $^{-3}$ and $P = 1.2483$ s from Sanidas et al. (2019), but obtained the best result – a narrow average pulse profile with $S/N > 7$ shown in Fig. 8 - with refined parameters of $P = 1.24827$ s (close to the initial one) and $DM = 17.124 \pm 0.020$ pc cm $^{-3}$, that is slightly bigger than the initial value. Our estimation of its scattering time constant $\tau_{sc} = 33 \pm 10$ ms.

PSR B0917+63. We used parameters $DM = 13.15423 \pm 0.00018$ pc cm $^{-3}$, and the period $P = 1.567994018$ s from Bilous et al. (2016) and Hobbs et al. (2004) for data processing, the prominent average pulse profile (Fig. 9) allowed us to obtain the $DM = 13.156 \pm 0.010$ pc cm $^{-3}$ and estimate the scattering time constant $\tau_{sc} = 15 \pm 8$ ms.

PSR J0928+30. Sanidas et al. (2019) give $DM = 21.95 \pm 0.09$ pc cm $^{-3}$ and $P = 2.0915$ s for this pulsar. With the optimal time of observations and the minimal RFI level, we found the average pulse profile at the detection limit with $S/N = 4$ (Fig. 10). However, it allowed us to measure the period $P = 2.09153$ s, and the $DM = 21.968 \pm 0.020$ pc cm $^{-3}$.

PSR J0935+33. The latest measured parameters of this pulsar as for the early 2020 were $P = 0.9615$ s, and $DM = 18.35 \pm 0.06$ pc cm $^{-3}$ in Sanidas et al. (2019). Using these parameters did not result in detection (see Fig. 11), but the period value tuning to the value $P = 0.96155$ s allowed us to find reliably the average pulse profile (Fig. 12) and to measure the $DM = 18.34 \pm 0.02$ pc cm $^{-3}$.

PSR J1303+38. Sanidas et al. (2019) give the $P = 0.3963$ s, and $DM = 19.000 \pm 0.009$ pc cm $^{-3}$ for this pulsar, but using these parameters also did not result in a detection, so we had to tune the period value. The rotation period $P = 0.39627$ s gave a weak average pulse profile near the detection limit (Fig. 13) which allowed us to measure the $DM = 19.012 \pm 0.020$ pc cm $^{-3}$.

PSR J1426+52. We have already shown this pulsar in Section 2 (see Fig. 2) as an example of period refinement, we found its $P = 0.995866$ s and $DM = 25.332 \pm 0.006$ pc cm $^{-3}$.

PSR J1628+4406. The discovery of this pulsar was reported in Lynch et al. (2018) with $DM = 7.32981 \pm 0.00002$ pc cm $^{-3}$ and

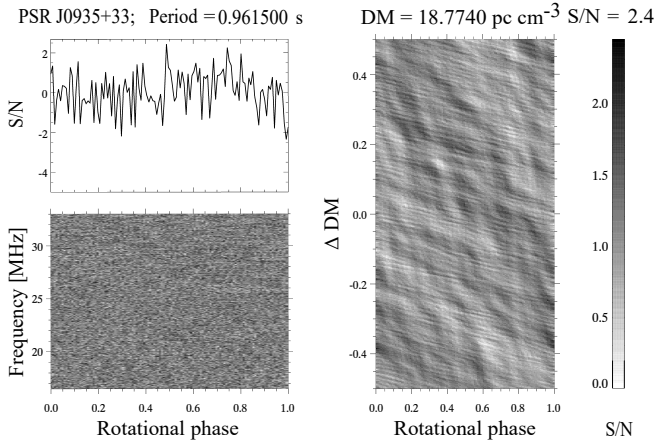


Figure 11. Unsuccessful detection of PSR J0935+33 on February 11, 2021 with rough DM = 18.35 ± 0.06 pc cm⁻³ and period $P = 0.9615$ s values.

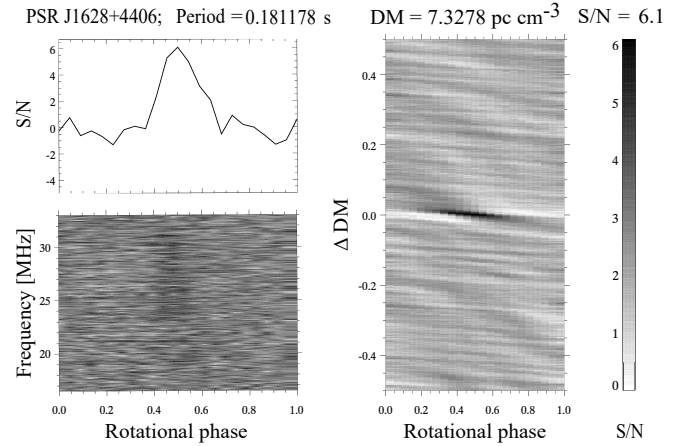


Figure 14. Detection of PSR J1628+4406 on May 26-27, 2020.

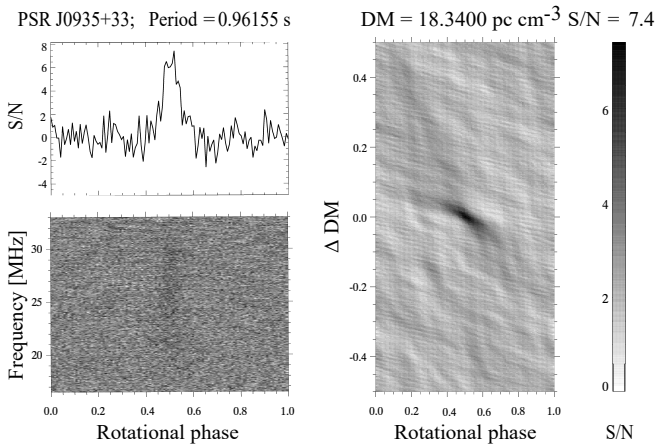


Figure 12. Detection of PSR J0935+33 on February 11, 2021 with the refined rotation period $P = 0.96155$ s.

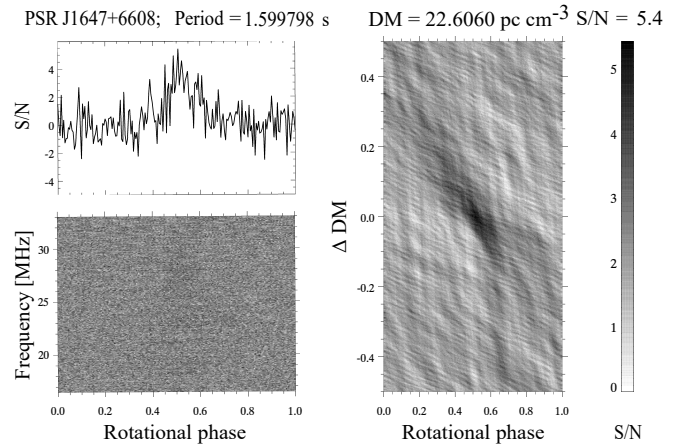


Figure 15. Detection of PSR J1647+6608 on September 8, 2020.

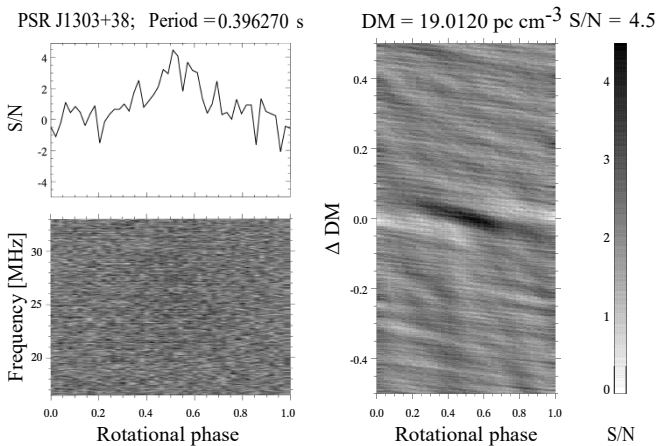


Figure 13. Detection of PSR J1303+38 on December 26, 2020 with the refined rotation period $P = 0.39627$ s.

$P = 0.18117848994714$ s. This accurate period value allowed us to reliably record the average pulse profile with the $S/N > 6$ (Fig. 14) and to estimate its $DM = 7.3278 \pm 0.0200$ pc cm⁻³. Since the period of PSR J1628+4406 is only 181 ms, it is the fastest pulsar detected on decametre waves so far.

PSR J1647+6608. The DM and rotation period of PSR J1647+6608 in Lynch et al. (2018) were estimated as 22.55 ± 0.07 pc cm⁻³ and 1.59979837535 s, respectively. We observed it in the evening of September 8, 2020 (culmination local time about 18h 00m) and detected it quite reliably with $S/N > 9$ (Fig. 15) which allowed us to estimate its $DM = 22.606 \pm 0.020$ pc cm⁻³.

PSR J1722+35 was observed in the afternoon of November 17, 2020 (culmination local time about 13h 00m). Sanidas et al. (2019) reports its $DM = 23.83 \pm 0.06$ pc cm⁻³ and $P = 0.8216$ s. Despite the low accuracy of period measurements, we detected this pulsar. The average pulse profile and parameters obtained with $P = 0.821616$ s, $DM = 23.902 \pm 0.020$ pc cm⁻³, are shown in Fig. 16.

PSR B2020+28. In Bilous et al. (2016) and Hobbs et al. (2004) its $DM = 24.63109 \pm 0.00018$ pc cm⁻³ and rotation period $P = 0.343402158$ s are given respectively. This pulsar like PSR J1628+4406 has a fairly short period of 343 ms, but it is still detectable at low frequencies (Fig. 17). Our estimate of its $DM = 24.642 \pm 0.020$ pc cm⁻³.

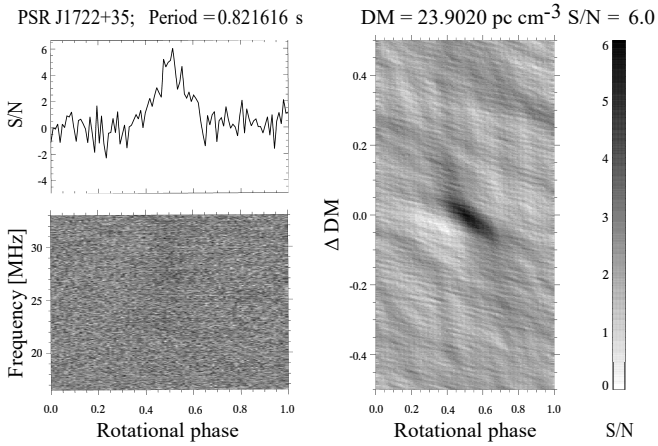


Figure 16. Detection of PSR J1722+35 on November 17, 2020 with the refined rotation period $P=0.821616$ s.

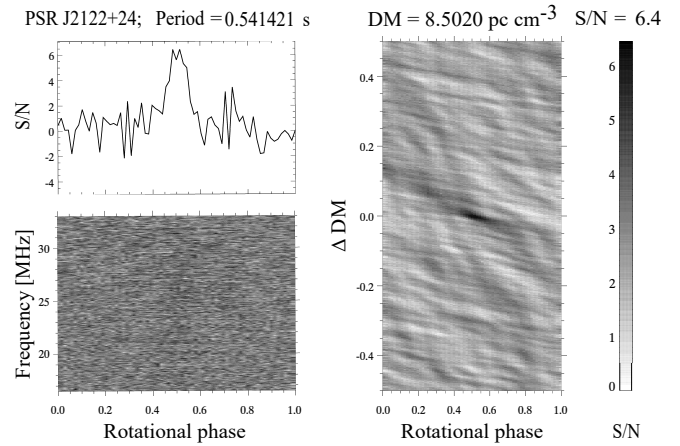


Figure 18. Detection of PSR J2122+24 on November 21, 2020.

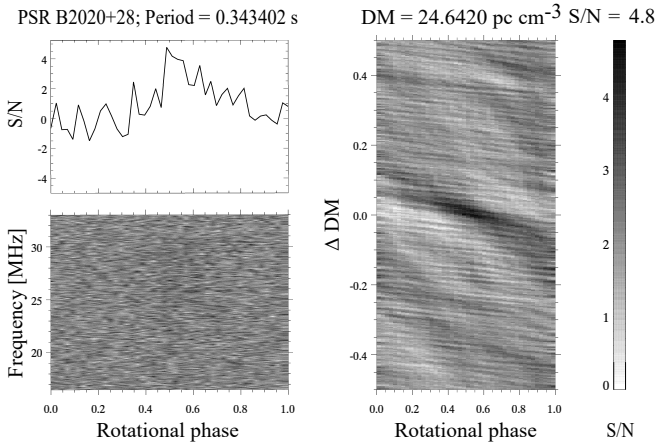


Figure 17. Detection of PSR B2020+28 on June 1, 2020.

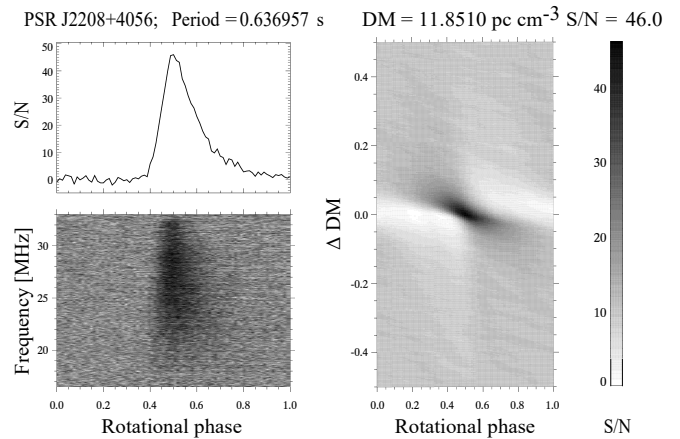


Figure 19. Detection of PSR J2208+4056 on February 14, 2020.

PSR J2122+24 was observed in September and November 2020. Its parameters in [Tan et al. \(2020\)](#) are: $DM = 8.500 \pm 0.005 \text{ pc cm}^{-3}$ and $P = 0.54142115903$ s. It was best detected on November 21, 2020 when its culmination was at approximately 16:50 local time, the average pulse profile is shown in Fig. 18. Our measured $DM = 8.502 \pm 0.020 \text{ pc cm}^{-3}$.

PSR J2208+4056 is the source with the highest $S/N=46$ obtained during the census. In [Lynch et al. \(2018\)](#) the estimates of its parameters are: $DM = 11.837 \pm 0.009 \text{ pc cm}^{-3}$, $P = 0.63695739361$ s. We observed it on February 14, 2020 in the afternoon (culmination local time about noon). Despite the daytime observations, it was detected reliably (Fig. 19) and our estimate of its $DM = 11.851 \pm 0.006 \text{ pc cm}^{-3}$, which is close to the previous estimates. The scattering time constant of this pulsar is $\tau_{sc} = 68 \pm 8$ ms.

PSR J2227+30. We observed it on February 9, 2020 in the afternoon (culmination was about 12:40 local time). The $DM = 19 \pm 2 \text{ pc cm}^{-3}$ is given in [Tyul'bashev et al. \(2018\)](#) and the period $P = 0.842408$ s we took from [Camilo et al. \(1996\)](#). Processing of data with these parameters did not give positive result which is well illustrated with the plots of DM value refining procedure in a DM range of 1 pc cm^{-3} shown in Fig. 20. However, in the right panel the upper left corner a part of a black oval is visible. Wide-range DM search-

ing in our pipeline allowed to detect *PSR J2227+30* quite reliably (Fig. 21). Our measurements gave the $DM = 19.972 \pm 0.020 \text{ pc cm}^{-3}$, which is 0.972 pc cm^{-3} bigger than specified in [Tyul'bashev et al. \(2018\)](#), but within its error interval. In a situation with a high influence of RFI and a narrow relative observation bandwidth, the accuracy of the DM value measurement in low-frequency studies (at least in the decametre and metre wave ranges) is much lower.

PSR J2325-0530 was observed in February and September 2020. In [Karako-Argaman et al. \(2015\)](#) its parameters are estimated as: $DM = 14.966 \pm 0.007 \text{ pc cm}^{-3}$, $P = 0.868735115026$ s. In the second observation session on September 7, 2020, it was detected most reliably (Fig. 22) because of night-time observations (culmination about 0:50 local time). The obtained $DM = 14.958 \pm 0.020 \text{ pc cm}^{-3}$ practically equals to the value given in [Karako-Argaman et al. \(2015\)](#).

PSR J2336-01 was observed on February 15, 2020 in the afternoon (culmination about 13:30 local time). Its parameters in [Sanidas et al. \(2019\)](#) were not accurate enough: $DM = 19.60 \pm 0.09 \text{ pc cm}^{-3}$, rotation period $P = 1.0298$ s. Although we detected the radiation of this pulsar even using this period value, we refined this parameter to $P = 1.0298454$ s, which resulted in measurement of $DM = 19.624 \pm 0.020 \text{ pc cm}^{-3}$ (Fig. 22).

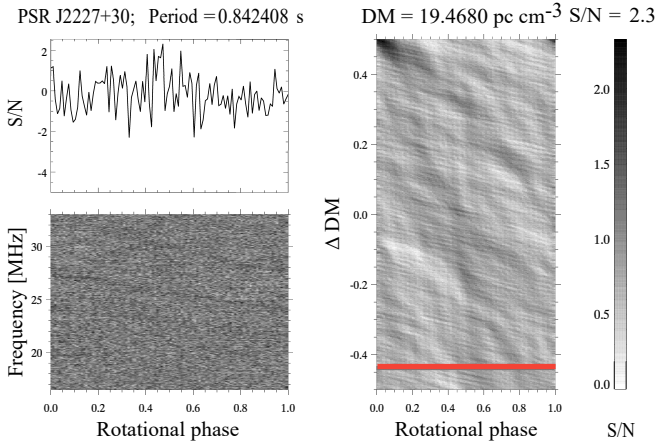


Figure 20. Unsuccessful detection of PSR J2227+30 on February 9, 2020 with the DM value from Tyul’bashev et al. (2018) (DM from the paper is indicated with the red line).

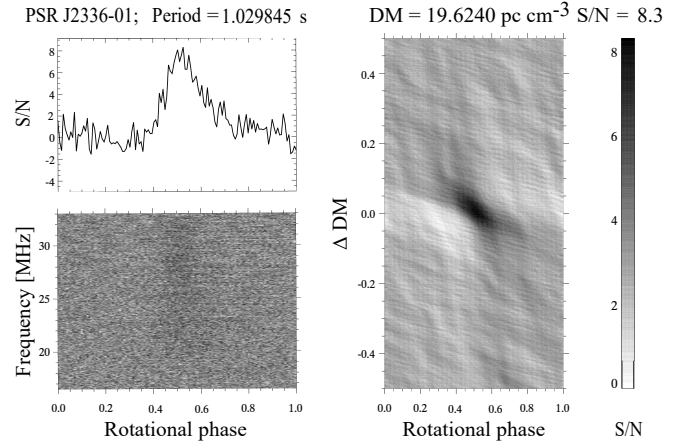


Figure 23. Detection of PSR J2336-01 on February 15, 2020 with the specified period $P = 1.0298454$ s.

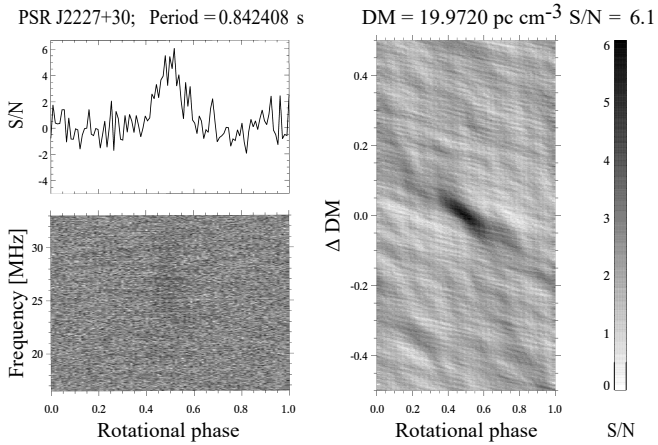


Figure 21. Detection of PSR J2227+30 on February 9, 2020 with the refined DM value.

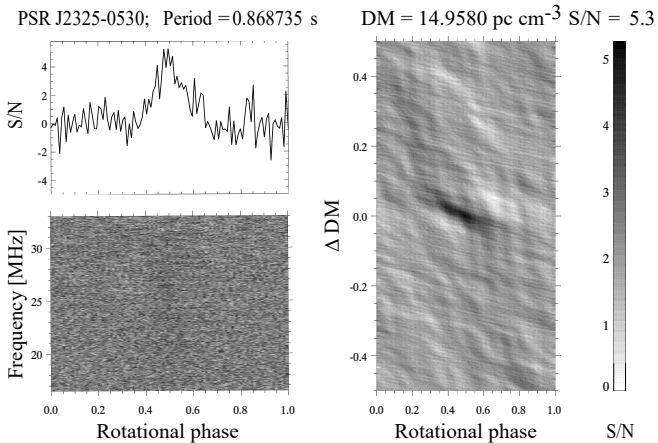


Figure 22. Detection of PSR J2325-0530 on September 7, 2020.

3.2 Analysis, discussion and prospects

In order to demonstrate more clearly our refinement of the DM of a number of pulsars, we have summarized them all in Table 1. The sixth column shows the target DM values for each pulsar obtained at higher frequencies, the seventh one – our DM values.

Note the pulsars detected with high enough S/N in which the DMs measured in this work differ significantly from those measured at high frequencies. For pulsars PSR J0121+14, PSR J0811+37, PSR J1426+52, PSR J1722+35, PSR B2020+28, PSR J2208+4056, PSR J2227+30, PSR J2325-0530, PSR J2336-01 the DM accuracy obtained in this work is rather high, so the new DM values for these pulsars are quite reliable. Flux densities and FWHM for each pulsar are also indicated in the table. The estimation error of flux densities as in Zakharenko et al. (2013) equals to 50%.

For six reliably detected pulsars, we estimated their scattering time constant (see Table 2). The scattering time constant of all detected pulsars is much less than their period and it is the main feature which allows us to distinguish the on-pulse component against the background of off-pulse. If τ_{sc}/P ratio is close to 1, the detection is significantly more difficult, because in this case the differences between the on-pulse and off-pulse components levels depend on the scattering of the pulse. So far, we can state that all pulsars with DM values, at least, up to 30 pc cm^{-3} should be well detectable at decametre waves because the on-pulse and off-pulse components are well distinguishable in case of enough sensitivity.

In Table 3 the upper limits (at 4σ level) of flux densities of 102 not yet detected pulsars in assumption that they have 10% duty cycle (pulse duration to pulsar period ratio) are given.

In this study, we found decametre radio emission of 20 pulsars, thus, their total number in this wave range reached 63 for now. The left panel of Fig. 24 shows all 20 detected pulsars mapped to the celestial sphere, the right one – 102 not yet detected pulsars of the selected parameter range. Fig. 25 shows the histogram of galactic latitudes distribution of already detected and not yet detected pulsars. In decametre wave range, galactic background brightness temperature is very high, which significantly complicates the detection of pulsars. As one can see from Fig. 24, about 2/3 of the 122 sought pulsars are located in rather cold regions of the sky. We obtained approximately the same ratio for the 20 newly detected sources. At the same time, this may indicate that the regions far from the Galactic plane have

Table 1. Flux densities, rough (from previous works) and our refined dispersion measures and other parameters for twenty pulsars detected in decameter wave range in this work.

N	PSR name	Gl [°]	Gb [°]	JD	«Aim» DM [pc cm ⁻³]	Refined DM [pc cm ⁻³]	Flux [mJy]	FWHM [ms]
1	J0121+1	134.023	-47.946	2458890.000000	17.77(9)	17.690(20)	22±11	78±8
2	B0301+19	161.135	-33.27	2458885.0868056	15.65677(35)	15.659(20)	4.7±2.4	
3	J0317+13	168.763	-36.04	2458896.0666782	12.90(4)	13.148(20)	6.1±3.1	
4	J0454+45	160.719	1.212	2459254.1541898	20.834(2)	20.854(20)	27±14	
5	J0613+3731	175.336	9.239	2459172.4285532	18.990(12)	18.986(20)	20±10	72±8
6	J0811+37	183.676	31.217	2458889.2889005	16.95(11)	17.124(20)	5.8±2.9	70±8
7	B0917+63	151.431	40.725	2458998.0402894	13.15423(18)	13.156(10)	13±7	98±8
8	J0928+30	195.838	45.915	2459255.3506944	21.95(9)	21.968(20)	3.6±1.8	
9	J0935+33	192.376	47.511	2459257.3396065	18.35(6)	18.34(20)	6.6±3.3	73±8
10	J1303+38	111.027	78.636	2459209.6177662	19.000(9)	19.012(20)	9±4.5	
11	J1426+52	93.88	59.233	2458885.5596644	25.37(2)	25.332(6)	34±17	88±8
12	J1628+4406	69.239	43.616	2458996.3402778	7.32981(2)	7.327(200)	6.9±3.5	
13	J1647+6608	97.18	37.034	2459101.0666782	22.55(7)	22.606(20)	15±8	
14	J1722+35	59.218	32.651	2459170.9000116	23.83(6)	23.876(20)	18±9	
15	B2020+28	68.863	-4.671	2459001.5048148	24.63109(18)	24.642(20)	24±12	
16	J2122+24	73.79	-17.973	2459175.0562616	8.500(5)	8.502(20)	24±12	
17	J2208+4056	92.574	-12.112	2458893.8576505	11.837(9)	11.851(6)	214±107	101±8
18	J2227+30	89.656	-22.815	2458888.8847222	19(2)	19.972(20)	16±8	
19	J2325-0530	75.579	-60.2	2459100.3459259	14.966(7)	14.958(20)	19±10	
20	J2336-01	84.424	-59.008	2459171.1598495	19.60(9)	19.624(20)	47±24	202±16

Table 2. Parameters of pulsars with estimated the scattering time constant τ_{sc} in decameter wave range.

N	PSR name	DM [pc cm ⁻³]	S/N	τ_{sc} [s]	P [s]	τ_{sc}/P
1	J0121+14	17.690(20)	16.2	0.051(16)	1.388993	0.0367
2	J0613+3731	18.986(20)	26.2	0.030(10)	0.619198181	0.0484
3	J0811+37	17.124(20)	26.4	0.033(10)	1.24827	0.0264
4	B0917+63	13.156(10)	14.8	0.015(8)	1.567994018	0.00957
5	J1426+52	25.332(6)	18.1	0.053(16)	0.995866	0.0532
6	J2208+4056	11.851(6)	46	0.058(8)	0.636957394	0.107

not been studied thoroughly enough. It means that we can expect new discoveries of nearby pulsars mainly in these regions.

At low frequencies, due to the wide beam of UTR-2 antenna cross-shaped pattern in the summation mode we use to search for pulsars, the antenna side lobes capture the "hot" regions of the sky. And one of the methods to reduce the noise level when observing near "hot" areas is using antenna pattern with non-rectangular current distribution between the UTR-2 sections, which reduces the side lobes, and which is the aim of our future work.

Many pulsars we are tried to detect at decametre waves were discovered recently, so their timing needs improvement. As shown above, an inaccurate pulsar period is often an obstacle to its reliable detection in the low-frequency wave range. Therefore, we have improved our pulsar data processing and analysis routines and now they allow us to vary in a wide range both the pulsar rotation period and its dispersion measure. This processing pipeline will probably help us to discover the sources of repetitive radio emission (pulsars and RRATs) from the data of the first decametre survey of the Northern sky (Vasylieva et al. 2013; Vasylieva 2015; Kravtsov et al. 2016a,b,c; Zakharenko et al. 2018).

4 CONCLUSIONS

The main result of the second decametre pulsar census is the discovery of low-frequency radio emission from 20 sources and the

refinement of their radio emission parameters. The exact dispersion measure values will probably make it possible to identify some of the transient signals detected in the decametre wave range. A wide range of galactic latitudes, in which a significant number of the new pulsars were discovered, as well as rather high flux densities of some of them, give us a hope that further studies in the entire range of galactic latitudes at low frequencies will not be fruitless. This is also evidenced by the rapid (more than doubled in 10 years) increase in the number of newly discovered pulsars with a dispersion measure of up to 30 pc cm⁻³. Therefore, planning and making new surveys in the entire galactic latitudes range, as well as increasing the sensitivity of such observations, is an urgent task especially at low frequencies. The ways for solving the last of the aforementioned problems are increasing of the observation time, improving algorithms of RFI mitigation and searching for both periodic and single cosmic pulsed signals. It will make possible to advance in understanding the population of neutron stars in the nearest galactic surroundings, as well as in understanding the processes of their formation and emission.

ACKNOWLEDGEMENTS

This work is supported by a Grant for Research of Young Scientists of the NAS of Ukraine (2019-2020), a Grant of the NAS of Ukraine for Research Laboratories/Groups of Young Scientists of the NAS

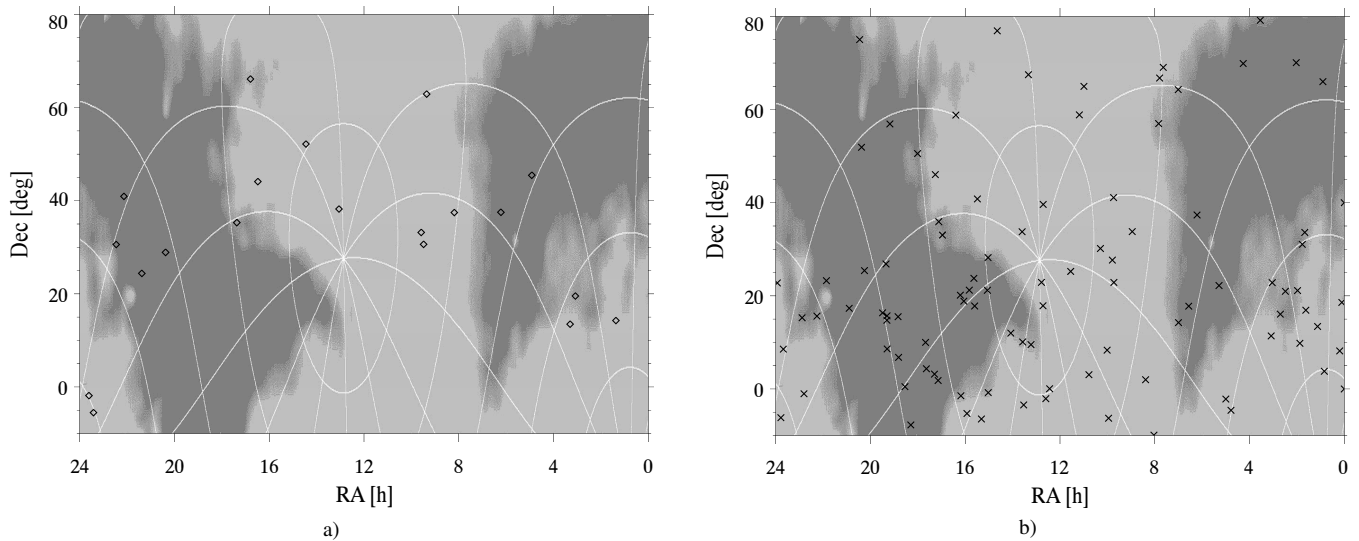


Figure 24. A map of the celestial sphere with twenty pulsars detected in this work (black stars, a) and 102 not yet detected pulsars with the parameters selected for the census (black crosses, b). Positions of the pulsars are overlapped on the northern sky map at 20 MHz (Sidorchuk et al. 2008)

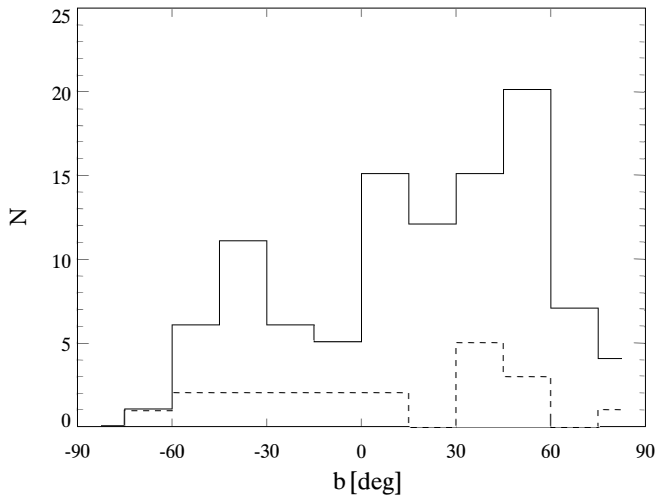


Figure 25. Galactic latitudes distribution histogram of detected (dashed line) and undetected pulsars (solid line). Each bin spans 15° on x-axis range from -90° to 90° .

of Ukraine (2020-2021), as well as the Latvian State Fellowship for Research (2020).

DATA AVAILABILITY

The data underlying this paper will be shared on reasonable request to the corresponding author.

REFERENCES

Bailes M., et al., 2017, *Publ. Astron. Soc. Aust.*, 34, e045
 Bilous A. V., et al., 2016, *A&A*, 591, A134
 Camilo F., Nice D. J., Shrauner J. A., Taylor J. H., 1996, *ApJ*, 469, 819
 Hewish A., Bell S. J., Pilkington J. D. H., Scott P. F., Collins R. A., 1968, *Nat*, 217, 709

Hobbs G., Lyne A. G., Kramer M., Martin C. E., Jordan C., 2004, *MNRAS*, 353, 1311
 Karako-Argaman C., et al., 2015, *ApJ*, 809, id. 67
 Kawash A. M., et al., 2018, *ApJ*, 857, 131
 Keane E. F., et al., 2014, in *Advancing Astrophysics with the Square Kilometre Array*. p. 20
 Konvalenko A., et al., 2016, *Exp. Astron.*, 42, 11
 Kravtsov I. P., Zakharenko V. V., Vasylieva I. Y., Ulyanov O. M., Shevtsova A. I., Skoryk A. O., Mykhailova S. S., 2016a, in *2016 9th International Kharkiv Symposium on Physics and Engineering of Microwaves, Millimeter and Submillimeter Waves (MSMW)*. pp 1–4
 Kravtsov I. P., et al., 2016b, *Adv. Astron. Space Phys.*, 6, 79
 Kravtsov I. P., et al., 2016c, *Odessa Astron. Publ.*, 29, 179–183
 Kravtsov I. P., et al., 2020, *Radio Phys. Radio Astron.*, 25, 193
 Lawson K. D., Mayer C. J., Osborne J. L., Parkinson M. L., 1987, *MNRAS*, 225, 307–327
 Lynch R. S., et al., 2018, *ApJ*, 859, 93
 Manchester R. N., Hobbs G. B., Teoh A., M. H., 2005, *ApJ*, 129, 1993
 Michilli D., et al., 2020, *MNRAS*, 491, 725
 Sanidas S., et al., 2019, *A&A*, 626, A104
 Sidorchuk M. A., Ulyanov O. M., Shepelev V. A., Mukha D. V., Brazhenko A. I., Vashchishin R. V., V. F. A., 2008, in *Scientific Workshop—Astrophysics with E-LOFAR* (DOI: 10.13140/RG.2.2.28090.82881).
 Stovall K., et al., 2015, *ApJ*, 808, 156
 Tan C. M., et al., 2020, *MNRAS*, 492, 5878–5896
 Tyul'bashev S. A., et al., 2018, *Astron. Rep.*, 62, 63–71
 Ulyanov O. M., Zakharenko V. V., Konvalenko A. A., Lecacheux A., Rosolen C., Rucker H. O., 2006, *Radio Phys. Radio Astron.*, 11, 113
 Ul'yanov O., Zakharenko V., 2012, *Astron. Rep.*, 56, 417–429
 Vasylieva I., 2015, PhD thesis, Observatoire de Paris
 Vasylieva I. Y., Zakharenko V. V., Zarka P., Ulyanov O. M., Shevtsova A. I., Seredkina A. A., 2013, *Odessa Astron. Publ.*, 26, 159
 Vasylieva I. Y., Zakharenko V. V., Konvalenko A. A., Zarka P., Ulyanov O. M., Shevtsova A. I., Skoryk A. O., 2014, *Radio Phys. Radio Astron.*, 19, 197
 Zakharenko V., et al., 2013, *MNRAS*, 431, 3624–3641
 Zakharenko V., et al., 2016, *JAI*, 5, id. 1641010
 Zakharenko V. V., Kravtsov I. P., Vasylieva I. Y., Konvalenko A. A., Ulyanov O. M., Kolyadin V. L., 2018, *Radio Phys. Radio Astron.*, 23, 79
 Zarka P., et al., 2015, in *2015 International Conference on Antenna Theory and Techniques (ICATT)*. pp 1–6

Table 3. The upper limits of flux density (4σ) of non-detected in this work pulsars.This paper has been typeset from a \LaTeX file prepared by the author.

N	Pulsar	Flux [mJy] (25 MHz)	N	Pulsar	Flux [mJy] (25 MHz)
1	J0006+1834	≤ 39	52	J1332-03	≤ 45
2	J0011+08	≤ 44	53	J1334+10	≤ 50
3	J0050+03	≤ 45	54	J1336+33	≤ 29
4	J0054+66	≤ 66	55	J1340+65	≤ 48
5	J0107+13	≤ 41	56	J1404+1159	≤ 53
6	J0137+1654	≤ 41	57	J1439+76	≤ 36
7	J0139+33	≤ 40	58	J1501-0046	≤ 60
8	J0146+31	≤ 39	59	J1502+28	≤ 40
9	J0152+0948	≤ 44	60	BJ1503+2111	≤ 56
10	J0158+21	≤ 40	61	JJ1518-0627	≤ 68
11	J0201+7005	≤ 61	62	J1529+40	≤ 31
12	J0215+51	≤ 88	63	J1536+17	≤ 66
13	J0229+20	≤ 40	64	J1538+2345	≤ 52
14	J0241+16	≤ 43	65	J1549+2113	≤ 60
15	J0302+22	≤ 40	66	J1555-0515	≤ 73
16	J0305+11	≤ 44	67	J1603+18	≤ 67
17	J0332+79	≤ 48	68	J1611-01	≤ 75
18	B0410+69	≤ 41	69	J1612+2008	≤ 64
19	J0447-04	≤ 48	70	J1623+58	≤ 33
20	J0459-0210	≤ 47	71	J1657+33	≤ 42
21	J0517+2212	≤ 51	72	J1703+00	≤ 96
22	B0609+37	≤ 42	73	J1707+35	≤ 41
23	J0633+1746	≤ 49	74	J1708+02	≤ 101
24	B0656+14	≤ 46	75	J1715+46	≤ 34
25	B0655+64	≤ 36	76	J1717+03	≤ 107
26	J0738+6904	≤ 35	77	J1726+34	≤ 66
27	J0747+6646	≤ 34	78	J1738+04	≤ 62
28	J0750+57	≤ 32	79	J1740+1000	≤ 106
29	J0802-09	≤ 54	80	J1800+5034	≤ 38
30	J0815+4611	≤ 46	81	J1817-0743	≤ 176
31	B0820+02	≤ 37	82	J1832+0029	≤ 149
32	J0857+33	≤ 23	83	J1848+0647	≤ 136
33	J0943+2253	≤ 25	84	J1850+15	≤ 101
34	J0944+4106	≤ 21	85	J1910+56	≤ 50
35	J0947+2740	≤ 24	86	J1917+0834	≤ 127
36	J0957-06	≤ 39	87	B1916+14	≤ 102
37	J1000+08	≤ 30	88	J1918+1541	≤ 98
38	J1011+18	≤ 38	89	B1918+26	≤ 73
39	J1017+30	≤ 24	90	J1929+16	≤ 95
40	J1046+0304	≤ 33	91	J2015+2524	≤ 75
41	J1049+5822	≤ 40	92	B2021+51	≤ 63
42	J1059+6459	≤ 29	93	J2027+7502	≤ 53
43	J1110+58	≤ 25	94	J2053+1718	≤ 72
44	J1132+25	≤ 29	95	J2151+2315	≤ 55
45	J1226+00	≤ 47	96	J2215+1538	≤ 53
46	J1235-02	≤ 49	97	J2248-0101	≤ 54
47	J1242+39	≤ 26	98	J2253+1516	≤ 47
48	J1243+17	≤ 38	99	J2340+08	≤ 46
49	J1246+2253	≤ 34	100	J2346-0609	≤ 54
50	J1313+0931	≤ 48	101	J2354+40	≤ 44
51	J1320+67	≤ 32	102	J2355+2246	≤ 39